Scientific Research Publishing

Atmospheric and Climate Sciences, 2023, 13, 341-352
https://www.scirp.org/journal/acs
ISSN Online: 2160-0422
ISSN Print: 2160-0414

Modeling Daily Average Temperatures in a Coastal Site of Central Africa: An Analysis of Seasonal Divisions

Jean-Pierre Bell[1], Esther C. Modi-Mbog[1,2], Nicodeme Djiedeu[1,3], Laurent Nana[1]

[1]Department of Physics, Faculty of Science, University of Douala, Douala, Cameroon
[2]Department of National Meteorology, Ministry of Transport, Yaoundé, Cameroon
[3]CEPAMOQ, Ecoles Doctorales, University of Douala, Douala, Cameroon
Email: jpbellfr@yahoo.fr, djienico@yahoo.fr

How to cite this paper: Bell, J.-P., Modi-Mbog, E.C., Djiedeu, N. and Nana, L. (2023) Modeling Daily Average Temperatures in a Coastal Site of Central Africa: An Analysis of Seasonal Divisions. *Atmospheric and Climate Sciences*, **13**, 341-352.
https://doi.org/10.4236/acs.2023.133019

Received: April 18, 2023
Accepted: July 2, 2023
Published: July 5, 2023

Abstract

The seasonality and day-to-day variation of near-surface temperature patterns can greatly control nearly all physical and biological processes though temperature predictions at such scales remain challenging. This paper implements a simple analytical approach in order to generate daily average temperatures which implicitly accounts for surface heating and drivers through a comprehensive representation of station-based temperature records on a universal standard calendar propagated by the earth's dynamics features. The modeled and observed pattern of daily temperatures exhibits a close agreement with the level of strength agreement exceeding 0.56. The extreme high and low values of the observed temperature patterns are equally well captured although model underestimates the probability of temperatures around the two modal peaks (~25.6˚C and 27.5˚C). Additionally, a theoretical thermal-based division led to the identification of six seasons, including two hot and cold periods along with two pairs of mixed hot-cold. The theoretical division proposed here appears to be a good approximation for the understanding of rainfall seasonality in this area.

Keywords

Daily Temperature Estimates, Earth's Dynamics, Seasonal Divisions

1. Introduction

Near-surface temperature is considered as one of the most prominent environmental parameters, playing a critical role for both weather conditions and natural systems; human lives and activities. Any variation in surface-air temperature

can affect processes related to the formation of rainfall, cloud and local circulation, which, along with temperature pattern control nearly all physical and biological processes. Plants productivity and growth, natural habitat and biodiversity, food cropping and human comfort are all very responsive to temperature variations from the daily to annual-term scales. Although atmospheric temperature information is of the utmost relevance for a wide range of practical applications, significant limitations in station-based observations in many areas of sub-Saharan Africa countries are still denoted, raising the prospect of enhanced demand in air temperature estimates for planning and informed decision making at the local scale.

Estimates of air temperature can be derived both from remote sensing and ground station based products. Among satellite remote sensing derived environmental parameters, Land Surface Temperatures (LSTs) have widely been associated with regional estimates of surface air temperature. If the spatial coverage of LST-induced air temperatures appears to be of great importance for regional impact assessments, existing LSTs over many regions are still poorly correlated with air temperatures (e.g. [1] [2] [3]). In a recent study which examined the different measures of urban heat intensity using both ground-based air temperatures and Landsat LSTs over China, Sheng *et al.* [4] found that the calculated urban heat intensity using the both datasets is not comparable suggesting that, there is no meaningful relationships of both data in their study. Additionally, areas with large vegetation and cloud coverage such as central Africa are likely to yield comparable poor correlation which might significantly worsen the skills of the induced air temperature estimates [5] [6] [7]. When compared with satellite retrieval, meteorological stations settled locally can record measurements of air temperature with high accuracy and temporal resolution. This is a prerequisite for skillful temperature estimates irrespective of the other dynamics processes to be considered.

At the near surface, air temperature is controlled by surface radiation budget through a partitioning into its turbulent heat fluxes. Heating at the surface mainly relies upon a number of features including surface physiography, weather parameters and the dynamics of the earth around the sun. Current predictions of temperatures are mostly conducted by modern numerical weather models (e.g. [8] [9]). These models are typically a physics-based representation of nonlinear and dynamics processes of the atmosphere, initialized by rapidly changing physio-graphical features and uncertain input weather observations. It emerges that considering this multitude of nonlinear dynamics processes and uncertain input in these models is likely one of the main sources of larger computing requirements and uncertainties, limiting their use for real-time applications. Moreover the time organizing system on which these models operate can also lead to additional uncertainties. Many evidences revealed that ordinary calendar systems cannot effectively account for variations in meteorological seasons which result from the combined effect of periodic and nonlinear land-ocean atmosphere response to the annual progression of the earth around the sun ([10] [11]). In such

time system the length of the meteorological season can range from 90 days for winter in non-leap year to 92 days for spring and summer.

A number of analytical approaches have been developed to generate weather variables, including parametric and deterministic methods. Most of these methods consist in an extensive analysis of long series of historical data from which model descriptors are extracted. While parametric methods consist in the determination of a few ensemble statistics allowing a good description of the overall behaviour, the existing explicit methods are more mathematical formulations based on a large number of Fourier series components of which coefficients do not always contain any significant meaning ([12] [13]). This study aims to propose an explicit-based approach to generate daily average temperatures based upon the description of the earth's dynamics allowing only a few number of model parameters. Thus, the objectives have been to: 1) extend the temperature modeling appraoch as previously introduced by N. Djiedeu [14] so as to account for the day-to-day variations; 2) determine how well the developed approach perform; 3) explore the setting of the developed analytical expression to propose a thermal-based seasonal division in this area. In the next section, we describe the modeling approach and the performance measures; the numerical results are presented and discussed in Section 3; and the final remarks provided in Section 4.

2. Materials and Methods

2.1. Modeling Approach of Daily Temperature over a Year

To theoretically describe the variation of monthly mean temperatures at a yearly basis, in a previous work by [14] it was established a sinusoidal function expressed as follows:

$$T(t) = a\sin\left[\omega_0(t)\right] + b\cos\left[\omega_0(t)\right] + c \tag{1}$$

where ω_0 is the Earth's frequency of revolution, c the annual mean temperature of the studied location. A nonlinear least square technique was used to fit the data obtained from meteorological measurements to the sinusoidal function.

In fact, the contributions of the Earth's revolution and the Earth's rotation are not observable on the curve of the monthly mean temperatures. We supposed that this could be observed on the curve of the daily mean temperatures. Therefore, a theory of perturbation was used to separate these contributions. The annual temperature being a constant for a given year, the perturbation only concerns the amplitude of the annual cycle. An expression of the temperature where the amplitude depend on the angular frequency of the Earth's rotation was used. This expression is then given as follow:

$$T(t) = \left[a_1\left(\cos^2\omega t\right) + a_2\right]\sin\omega_0 t + \left[a_3\left(\cos^2\omega t\right) + a_4\right]\cos\omega_0 t + a_5 \tag{2}$$

where ω is the Earth's frequency of rotation. Again, the nonlinear least square technique is used to fit the data obtained from meteorological measurements to the sinusoidal function.

2.1.1. Revolution Temperature and Rotation Temperature

The expression of the temperature in Equation (2) can be rewritten as:

$$\begin{aligned} T(t) &= \left[a_1\left(1-\sin^2\omega t\right)+a_2\right]\sin\omega_0 t+\left[a_3\left(1-\sin^2\omega t\right)+a_4\right]\cos\omega_0 t+a_5 \\ &= \left(a_1+a_2\right)\sin\omega_0 t-a_1\sin^2\omega t\sin\omega_0 t+\left(a_3+a_4\right)\cos\omega_0 t-a_3\sin^2\omega t\cos\omega_0 t+a_5 \\ &= \left(a_1+a_2\right)\sin\omega_0 t+\left(a_3+a_4\right)\cos\omega_0 t-\left(a_1\sin\omega_0 t+a_3\cos\omega_0 t\right)\sin^2\omega t+a_5 \\ &= T_{rev}(t)+T_{rot}(t) \end{aligned} \tag{3}$$

where

$$T_{rev}(t)=\left(a_1+a_2\right)\sin\omega_0 t+\left(a_3+a_4\right)\cos\omega_0 t+a_5 \tag{4}$$

and

$$T_{rot}(t)=-\left(a_1\sin\omega_0 t+a_3\cos\omega_0 t\right)\left(\sin\omega t\right)^2 \tag{5}$$

Note that the revolution temperature does not evolve with the angular frequency of the Earth's rotation while the rotation temperature fluctuate with both revolution and rotation frequencies.

2.1.2. Averaging of the Rotation Temperature

The mean of the rotation temperature can be calculated for any given value of interval. Let $\left\langle T_{rot}(t)\right\rangle$ be the mean of $T_{rot}(t)$:

$$\left\langle T_{rot}(t)\right\rangle=\frac{1}{T'}\int_{T_i}^{T_f}T_{rot}(t)\,\mathrm{d}t \tag{6}$$

where T_f and T_i are respectively the final and initial time of the chosen interval of time. $T'=T_f-T_i$ is the length or the duration of the period of time chosen. The linearization of $T_{rot}(t)$ and its substitution in Equation (6) leads to:

$$\begin{aligned} \left\langle T_{rot}(t)\right\rangle &= \frac{a_1}{4}\frac{1}{T'}\int_{T_i}^{T_f}\left[\sin\left(\omega_0+2\omega\right)t+\sin\left(\omega_0-2\omega\right)t\right]\mathrm{d}t \\ &\quad -\frac{a_1}{2}\frac{1}{T'}\int_{T_i}^{T_f}\sin\omega_0 t\,\mathrm{d}t+\frac{a_3}{4}\frac{1}{T'}\int_{T_i}^{T_f}\left[\cos\left(\omega_0+2\omega\right)t+\cos\left(\omega_0-2\omega\right)t\right]\mathrm{d}t \\ &\quad -\frac{a_3}{2}\frac{1}{T'}\int_{T_i}^{T_f}\sin\omega_0 t\,\mathrm{d}t \end{aligned} \tag{7}$$

The integration of Equation (7) leads to:

$$\begin{aligned} \left\langle T_{rot}(t)\right\rangle &= -\frac{a_1}{4T'}\left[\frac{1}{\omega_0+2\omega}\cos\left(\omega_0+2\omega\right)t+\frac{1}{\omega_0-2\omega}\cos\left(\omega_0-2\omega\right)t\right]_{T_i}^{T_f} \\ &\quad +\frac{a_3}{4T'}\left[\frac{1}{\omega_0+2\omega}\sin\left(\omega_0+2\omega\right)t+\frac{1}{\omega_0-2\omega}\sin\left(\omega_0-2\omega\right)t\right]_{T_i}^{T_f} \\ &\quad +\frac{a_1}{2\omega_0 T'}\left[\cos\omega_0 t\right]_{T_i}^{T_f}+\frac{a_3}{2\omega_0 T'}\left[\cos\omega_0 t\right]_{T_i}^{T_f} \end{aligned} \tag{8}$$

2.1.3. Daily Mean of Rotation Temperature

For a daily mean, we have:

$$T_f=T_i+T=\left(n+1\right)T \tag{9}$$

where $T=\frac{2\pi}{\omega}$ is the time period of earth's rotation and n the ranking of the day in a given year. We then have:

$$\begin{aligned}\left\langle T_{rot}(t)\right\rangle = &-\frac{a_1}{4\pi}\frac{\omega\omega_0}{\omega_0^2-4\omega^2}\left(\cos\frac{2\pi(n+1)}{365}-\cos\frac{2\pi n}{365}\right)\\ &+\frac{a_3}{4\pi}\frac{\omega\omega_0}{\omega_0^2-4\omega^2}\left(\sin\frac{2\pi(n+1)}{365}-\sin\frac{2\pi n}{365}\right)\\ &+\frac{365}{4\pi}(a_1+a_3)\left(\cos\frac{2\pi(n+1)}{365}-\cos\frac{2\pi n}{365}\right)\end{aligned} \tag{10}$$

using $\frac{\omega}{\omega_0}=365$, we obtain:

$$\begin{aligned}\left\langle T_{rot}(n+1)\right\rangle = &\frac{365}{5836}\frac{a_1}{\pi}\left(\cos\frac{2\pi(n+1)}{365}-\cos\frac{2\pi n}{365}\right)\\ &-\frac{365}{5836}\frac{a_3}{\pi}\left(\sin\frac{2\pi(n+1)}{365}-\sin\frac{2\pi n}{365}\right)\\ &+\frac{365}{4\pi}(a_1+a_3)\left(\cos\frac{2\pi(n+1)}{365}-\cos\frac{2\pi n}{365}\right)\end{aligned} \tag{11}$$

with $n\geq 0$. Finally, the mean value of the rotation temperature as a function of a day's ranking n is derived from Equation (12) as:

$$\begin{aligned}\left\langle T_{rot}(n)\right\rangle = &\frac{365}{5836}\frac{a_1}{\pi}\left(\cos\frac{2\pi n}{365}-\cos\frac{2\pi(n-1)}{365}\right)\\ &-\frac{365}{5836}\frac{a_3}{\pi}\left(\sin\frac{2\pi n}{365}-\sin\frac{2\pi(n-1)}{365}\right)\\ &+\frac{365}{4\pi}(a_1+a_3)\left(\cos\frac{2\pi n}{365}-\cos\frac{2\pi(n-1)}{365}\right)\end{aligned} \tag{12}$$

with $n\geq 1$.

2.1.4. Annual Mean of Rotation Temperature

Evaluated for one year that is for $T_i=0$ and $T_f=T_0=\frac{2\pi}{\omega_0}$ which is then the Earth's period of revolution, we obtain:

$$\left\langle T_{rot}(t)\right\rangle=\frac{a_1\omega_0^2}{4\pi\left(4\omega^2-\omega_0^2\right)}\cos\left(4\pi\frac{\omega}{\omega_0}\right)+\frac{a_3\omega\omega_0}{2\pi\left(4\omega^2-\omega_0^2\right)}\sin\left(4\pi\frac{\omega}{\omega_0}\right) \tag{13}$$

That is:

$$\left\langle T_{rot}(t)\right\rangle=\frac{a_1\omega_0^2}{4\pi\left(4\omega^2-\omega_0^2\right)}=\frac{a_1}{2131596\pi} \tag{14}$$

note that a_1 is generally a small value therefore the rotation temperature is weak. This parameter, which accounts for the contribution of the Earth's rotation to the daily mean temperature of a given location, is of small magnitude

compared to that of the revolution temperature. Although its small magnitude, this contribution is critical to capture the short-term and small magnitude variations.

2.2. *In Situ* Station-Based Observations and Performance Metrics

The *in situ* observations used in this study are daily average temperature data obtained from a synoptic meteorological station of the Douala international Airport, a coastal location of Cameroon in the central Africa region (Figure 1). These data along with other meteorological parameters are collected by the Agency for the Safety of Air Navigation in Africa and Madagascar (ASECNA), which the primary goal is the production of forecasting information related to the aviation meteorology.

To evaluate the skill of the proposed approach of predicted air temperatures, we used a feature-based similarity method which account for both the deterministic features covering the raw-value shape of the time series and the stochastic features representing the distributions. Thus, the model was assessed by the means of the following: root mean square difference (RMSD, absolute and relative values), scatterplots of the estimated values as a function of the observed ones, the probability density distributions, and the concordance correlation coefficient (ρ_c). The following expressions for RMSD (˚C and %: absolute and relative value) were used:

$$\mathrm{RMSD}(^{\circ}\mathrm{C}) = \left[\frac{1}{N}\sum_{i=1}^{N}\left(T_{i,mod} - T_{i,obs}\right)^2\right]^{1/2} \tag{15}$$

$$\mathrm{RMSD}(\%) = \frac{100}{\overline{T}_{obs}}\left[\frac{1}{N}\sum_{i=1}^{N}\left(T_{i,mod} - T_{i,obs}\right)^2\right]^{1/2} \tag{16}$$

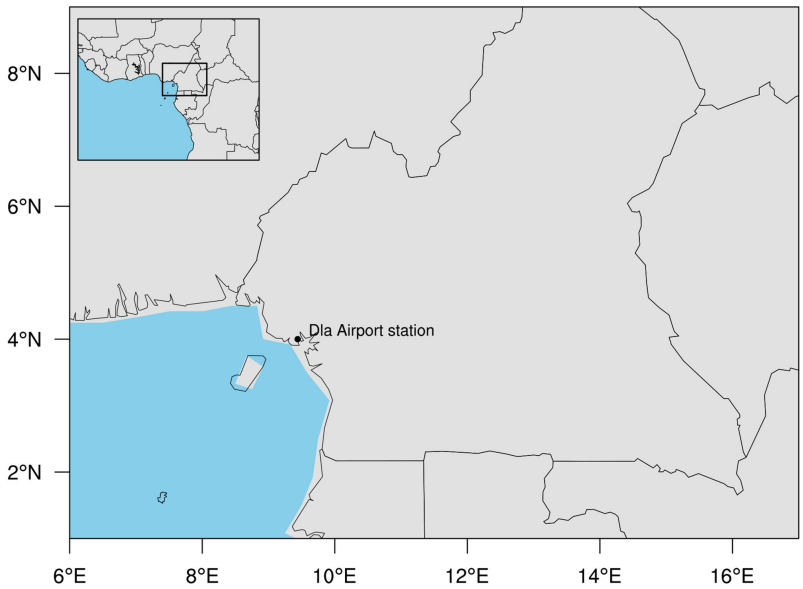

Figure 1. Map showing the location of the Douala International Airport weather station site.

where $T_{i,mod}$ is the modeled temperature value, N is the number of data points, $T_{i,obs}$ is the observed temperature value and $\overline{T}_{obs}$ is a long-term mean air temperaute value. In addition, ρ_c given a measure of the level of strength agreement is computed as follows:

$$\rho_c = \frac{2\sigma_{mod,obs}}{\sigma_{mod}^2 + \sigma_{obs}^2 + \left(\mu_{mod} - \mu_{obs}\right)^2} = \rho C_b \tag{17}$$

where μ_{mod} and μ_{obs} are the means of the observed and estimated temperatures while σ_{mod}^2 and σ_{obs}^2 represent the variances of the two temperatures series respectively. $\sigma_{mod,obs}$ indicates the cross correlation between the estimates and observations. ρ_c is also expressed as the product of the Pearson correlation coefficient (ρ) and the bias correction factor (C_b) which is computed as follows:

$$C_b = \left[\left(\frac{\sigma_{mod}}{\sigma_{obs}} + \frac{\sigma_{obs}}{\sigma_{mod}} + \frac{\left(\mu_{mod} - \mu_{obs}\right)^2}{\sigma_{mod}\sigma_{obs}}\right) \Big/ 2\right]^{-1} \tag{18}$$

The value of ρ_c is in the range between −1.0 and 1.0, it can be shown that $\rho_c = \pm 1$ if and only if $\rho = \pm 1$, $\sigma_{mod} = \sigma_{obs}$ and $\mu_{mod} = \mu_{obs}$. Thus, $\rho_c = 1$ (-1) if and only if $T_{i,mod} = T_{i,obs}$ $(-T_{i,obs})$ that is when there is perfect agreement (disagreement). The bias correction factor C_b $(0 \le C_b \le 1)$ in (18) assesses the level of bias, with smaller C_b indicating larger bias. Therefore, poor agreement can result from low correlation (small ρ) or large bias (small C_b).

3. Numerical Results

3.1. Modeled Daily Temperatures and Performance

Temperature estimates as generated by the newly developed approach is compared to *in situ* observations from 2000 to 2009 obtained from a local meteorological station. Figure 2 shows the multi-year daily observed temperatures superimposed by model estimates. In general, the modeled temperatures capture well the multi-years observed pattern although the day-to-day variation still exhibits some discrepancies. The most notable feature is during the 2004-2005 period when model fails to capture the observed pattern, showing considerable departure in magnitude between the simulated and observed temperatures. Note that during the 2004-2005 period tropical forested regions of the Amazon and Congo basins have experienced unusual climate conditions induced by a moderate El nino Southern oscillation (ENSO) event which generated drought conditions associated with lower rainfall and higher temperatures. This is, though, in constrast with the low temperatures measured in 2005 at the local station indicating that discrepancies during this period presumably hide a deficiency of the measuring system.

Regarding the scatter plot of the observed daily average temperatures as a function of estimates, the diagonal line represents the ideal match between the estimated and measured values. Figure 3 shows that over the entire integration

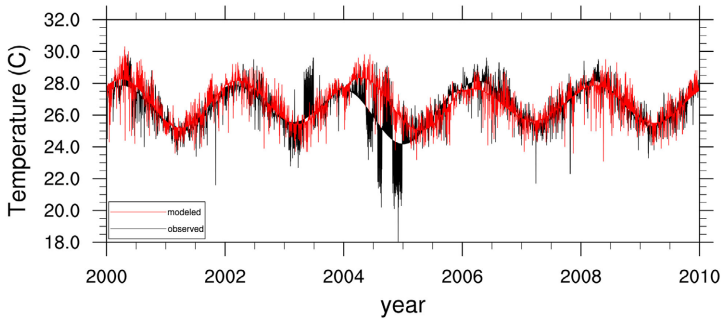

Figure 2. Pattern of daily average temperatures from both obervations and model. The black line represents the *in situ* data and the red line the model estimates.

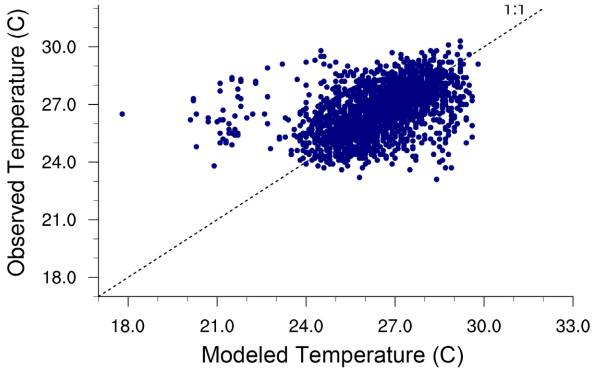

Figure 3. Scatterplot of the estimated daily temperatures against observations for the 2001-2010 period. The straight black line indicates the line of 45˚.

period the two sets quite well follow the line of 45˚, indicating that the overall relationships between the modeled and station-measured temperatures is reasonable.

At the yearly granularity, a set of indicators including root mean square error (RMSE) absolute and relative values, concordance correlation coefficient and bias were used to test and examine the performance of the developed approach. Table 1 indicates that for most of years the RMSE absolute result roughly varies from 0.73˚C to 1.17˚C except for the year 2004. Consistently, the RMSE relative value is ranging from 2.82% to 4.45% while reaching 9.68% in 2004. These values are quite lower compare to that obtained by [15] in a comparative assessment of air temperature models. Based on the minimum and maximum relative RMSE values, they show that among the models that calculate daily air temperature the standard model is the best ahead the CLIMEDTEM model with RMSE relative values ranging from 3.34% to 11.34% and 13.85% to 43.83% respectively. the year 2004 exhibits the highest relative RMSE value 9.68% coinciding with the smaller concordance coefficients ($\rho_c = 0.31$), indicating the worst level of agreement between the measured and Modeled temperatures. The smaller relative RMSE value depicted during the 2004 year points to the influence of variation of bias indicator ($C_b = 0.52$) on the level of strength agreement.

Table 1. Performance metrics for the simulated daily temperatures with respect to observations at a yearly basis. RMSD = Root mean square difference in ˚C and %, CCC (ρ_c) Concordance correlation coefficient.

	2000	2001	2002	2003	2004	2005	2006	2007	2008	2009
RMSD (˚C)	1.07	0.80	0.88	1.17	2.50	0.92	0.93	0.92	0.89	0.73
RMSD (%)	3.95	3.13	3.26	4.45	9.68	3.57	3.39	3.56	3.29	2.82
C_b	0.95	0.96	0.95	0.97	0.52	0.97	0.89	0.98	0.98	0.99
CCC(ρ_c)	0.61	0.74	0.61	0.56	0.31	0.69	0.57	0.57	0.65	0.79

To further evaluate the similarities of the two temperatures series, the probability distributions of the observed and modeled daily temperatures for 2001-2010 were illustrated in **Figure 4**. Probability density distribution of the observed temperatures exhibits two peaks approximately at the temperatures of 25.6˚C and 27.5˚C respectively. This bimodal pattern is quite well depicted by predicted temperatures although the model underestimates the probability between the modal values of the observed series.

3.2. Transition Dates and Seasonal Divisions

Derived and validated in sections 2 & 3, the analytical expression of the temparature is a continuous variable of time which allows an explicit determination of the different seasons over a year. We then need first of all to find the Transition dates between the different periods. There are only three considerations to be used: 1) when the second derivative of the temperature with respect to time vanishes, the time values obtained represent the transition dates between the hot and the cold periods, and reversely. At these dates, the seasonal progression of the temperature coincides with the annual mean temperature. 2) when the progression of the seasonal temperature coincides with the half maximum during the hot period, the obtained dates correspond either to the transition between the hot and the moderate hot 2 periods or the transtion between the hot and the moderate hot 1 periods associated with a negative or positive second differential of the temperature respectively. 3) when the annual temperature cycle coincides with the half maximum during the cold period, the derived dates correspond either to the transition between the cold and the moderate cold 1 period or the transition between the cold and the moderate cold 2 period associated with a negative or positive second derivative of the temperature respectively. A detailed description of the theoretical determination of transition dates was provided in [14]. This permits the identification of six thermal-based seasons including a hot and cold seasons along with two pairs of mixed hot-cold periods (**Table 2**). It should be noted that temperature plays a determinent role in the processes of rainfall formation over the Congo and Amazonia basins where local recycling can account for more 39% of rainfall ([16] [17]). Additionally, a recent study has established robust and strong correlations between increases in the temperature seasonal cycle and drying over the Amazonia basin [18]. This suggests that the

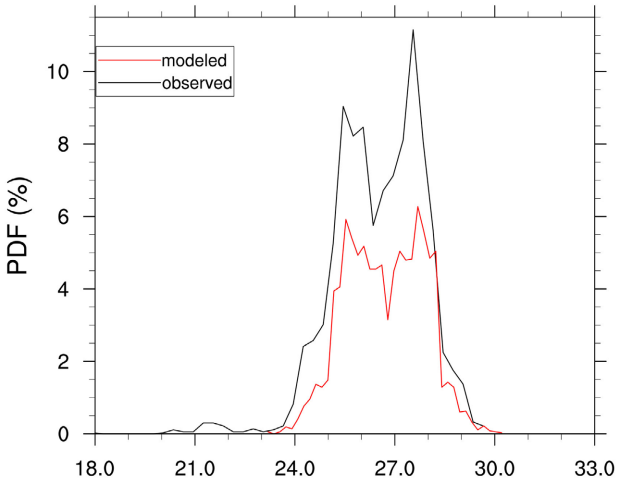

Figure 4. Probability density distribution of daily temperatures for the 10-year period (2001-2010). The solid red and black lines indicate the modeled and observed temperatures respectively.

Table 2. Seasonal divisions of the areas in the vicinity of the Douala airport site.

Period	December 8th to March 17th	March 17th to May 20th	May 20th to June 22nd	June 22nd to October 6th	October 6th to November 6th	November 6th to December 9th
Duration (month)	4.34	1.1	1.1	4.4	1.0	1.1
Season	hot period	Moderate hot 2	Moderate cold 1	Cold period	Moderate cold 2	Moderate hot 1

theoretical thermal-based division proposed here can be a good approximation for the understanding of rainfall seasonality.

4. Summary and Conclusions

An analytical approach was developed to generate daily temperature estimates at a yearly basis. The model contains an explicit description of pattern and variations of the daily average temperatures for a given location by the mean of a combined two-component of long and short term periodic functions. A ten years historical daily data were analyzed on a thirteen months calendar (universal standard calendar) and then the model descriptors were obtained by fitting the theoretical function to the historical temperatures. Daily average temperatures were then synthetisized for this location covering the same ten years period as the historical data. A set of performance measures were used to assess how well the model reproduces the observed station data.

Overall, the relationship between model and observations is reasonable. The generated temperatures capture well the multi-year observed pattern although the day-to-day variation still exhibits some discrepancies. Relative RMSE values vary from 2.82% to 4.45% which is quite well lower compared to that obtained in

a comparative assessment comprising multi analytical temperature models. The probability distribution of the generated temperatures is also similar to that of the climate being modeled. In addition, a theoretical thermal-based division led to the identification of six seasons, including two hot and cold periods along with two pairs of mixed hot-cold periods. The theoretical division proposed in this work appears to be a good approximation for the understanding of rainfall seasonality in this area.

This approach is powerful in that, by using the earth's dynamics features, it implicitly accounts for the others influencing factors of temperature. The approach is simple and requires only small computing effort. This points to the suitability of these results for real time applications over areas of low density observations, including for instance decision on how many or what mixed of seasonal products to manufacture and store; what crop if any to plant or what actions should be taken to prevent from vector-borne diseases such as malaria.

Acknowledgements

The authors wish to thank the Agency for the Safety of Air Navigation in Africa and Madagascar (ASECNA) for making the station-based temperature data freely available. The third author acknowledges support for this work from the Abdus Salam International Centre for Theoretical Physics (ICTP, Trieste Italy) under the OEA-12 projects.

Conflicts of Interest

The authors declare no conflicts of interest regarding the publication of this paper.

References

[1] Xiong, Y. and Chen, F. (2017) Correlation Analysis between Temperatures from Landsat Thermal Infrared Retrievals and Synchronous Weather Observations in Shenzhen, China. *Remote Sensing Applications*: *Society and Environment*, **7**, 40-48. https://doi.org/10.1016/j.rsase.2017.06.002

[2] Yang, Y.Z., Cai, W.H. and Yang, J. (2017) Evaluation of MODIS Land Surface Temperature Data to Estimate Near-Surface Air Temperature in Northeast China. *Remote Sensing*, **9**, Article No. 410. https://doi.org/10.3390/rs9050410

[3] Sun, T., Sun, R. and Chen, L. (2020) The Trend Inconsistency between Land Surface Temperature and near Surface Air Temperature in Assessing Urban Heat Island Effects. *Remote Sensing*, **12**, Article No. 1271. https://doi.org/10.3390/rs12081271

[4] Sheng, L., Tang, X., You, H., Gu, Q. and Hu, H. (2017) Comparison of the Urban Heat Island Intensity Quantified by Using Air Temperature and Landsat Land Surface Temperature in Hangzhou, China. *Ecological Indicators*, **72**, 738-746. https://doi.org/10.1016/j.ecolind.2016.09.009

[5] Vancutsem, C., Ceccato, P., Dinku, T. and Connor, S.J. (2010) Evaluation of MODIS Land Surface Temperature Data to Estimate Air Temperature in Different Ecosystems over Africa. *Remote Sensing*, **114**, 449-465. https://doi.org/10.1016/j.rse.2009.10.002

[6] Lian, X., Zeng, Z., Yao, Y. and Peng, S. (2017) Spatiotemporal Variations in the Difference between Satellite-Observed Daily Maximum Land Surface Temperature and Station-Based Daily Maximum Near-Surface Air Temperature. *Journal Geophysical Research*: *Atmospheres*, **122**, 2254-2268. https://doi.org/10.1002/2016JD025366

[7] Kambi, M.O.C., Wang, Z. and Gulemvuga, G. (2018) Determination of the Correlation between the Air Temperature Measured *in Situ* and Remotely Sensed Data from MODIS and SEVIRI in Congo-Brazzaville. *Atmospheric and Climate Sciences*, **8**, 192-211. https://doi.org/10.4236/acs.2018.82013

[8] Smith, D.M., Cusack, S., Colman, A.W., Folland, C.K., Harris, G.R. and Murphy, J.M. (2007) Improved Surface Temperature Prediction for the Coming Decade from a Global Climate Model. *Science*, **317**, 796-799. https://doi.org/10.1126/science.1139540

[9] Duan, H.X., Li, Y.H., Zhang, T.J., Pu, Z.X., Zhao, C.L. and Liu, Y.P. (2018) Evaluation of the Forecast Accuracy of Near-Surface Temperature and Wind in Northwest China Based on the WRF Model. *Journal of Meteorological Research*, **32**, 469-490. https://doi.org/10.1007/s13351-018-7115-9

[10] Pezzulli, S., Stephenson, D.B. and Hannanchi, A. (2005) The Variability of Seasonality. *Journal of Climate*, **18**, 71-88. https://doi.org/10.1175/JCLI-3256.1

[11] Stine, A.R. and Huybers, P. (2012) Changes in the Seasonal Cycle of Temperature and Atmospheric Circulation. *Journal of Climate*, **25**, 7362-7380. https://doi.org/10.1175/JCLI-D-11-00470.1

[12] Cuomo, V., Fontana, F. and Serio, C. (1986) Behaviour of Ambient Temperature on Daily Basis in Italian Climate. *Revue de Physique Appliquée*, **21**, 211-218. https://doi.org/10.1051/rphysap:01986002103021100

[13] Parrott, L., Kok, R. and Lacroix, R. (1996) Daily Average Temperatures: Modeling and Generation with a Fourier Transform Approach. *Transactions of the ASAE*, **39**, 1911-1922. https://doi.org/10.13031/2013.27670

[14] Djiedeu, N. (2017) Nature of Forces Acting on the Terrestrial Globe. LAP LAMBERT Academic Publishing, Saarbrücken, 66-82.

[15] Bilbao, J. and De Miguel, A.H. (2002) Air Temperature Model Evaluation in the North Mediterranean Belt Area. *Journal of Applied Meteorology*, **41**, 872-884. https://doi.org/10.1175/1520-0450(2002)041<0872:ATMEIT>2.0.CO;2

[16] Brubaker, K.L., Entekhabi, D. and Eagleson, P.S. (1993) Estimation of Continental Precipitation Recycling. *Journal of Climate*, **6**, 1077-1089. https://doi.org/10.1175/1520-0442(1993)006<1077:EOCPR>2.0.CO;2

[17] Theeuwen, J., Staal, A., Tuinenburg, O.A., Hamelers, B.V.M. and Dekker, S.C. (2022) Local Moisture Recycling across the Globe. EGUsphere, 1-20. https://doi.org/10.5194/egusphere-2022-612

[18] Ritchie, P.D.L., Parry, I., Clarke, J.J. and Huntingford, C. (2022) Increases in the Temperature Seasonal Cycle Indicate Long-Term Drying Trends in Amazonia. *Communications Earth & Environment*, **3**, Article No. 199. https://doi.org/10.1038/s43247-022-00528-0